Ultrametricity property of energy landscapes of multidisperse packing problems

Johannes J. Schneider,* André Müller,† and Elmar Schömer‡
Department of Physics, Mathematics, and Computer Science, Johannes Gutenberg University of Mainz, Staudinger Weg 7, 55099 Mainz, Germany

(Received 27 December 2008; published 26 March 2009)

We consider the problem of finding the densest closed packing of hard disks with proposed different radii in a circular environment, such that the radius of the circumcircle is minimal. The subspace of the quasioptimum configurations of this problem exhibits the property of ultrametricity.

DOI: 10.1103/PhysRevE.79.031122 PACS number(s): 64.60.De, 64.75.Gh, 65.40.Ba, 89.75.Da

I. INTRODUCTION

Recently, a benchmark for the problem of finding the densest closed packing of a multidisperse system of hard disks was defined as follows [1]: consider a system of N hard disks with successive integer radii $r_i=i$ $(i=1,2,\ldots,N)$. These disks are to be packed in a circular environment in a way that the radius R of the circumcircle is minimized and that the various disks must not overlap. In the benchmark contest, only small system sizes $5\leq N\leq 50$ were considered. The best solution we found for 50 disks is shown in Fig. 1. If denoting the coordinates of the midpoint of disk i as x_i and y_i and assuming the midpoint of the circumcircle to be located at the origin, the Hamiltonian of the problem can be rewritten as

$$R=\max_i(\sqrt{x_i^2+y_i^2}+r_i). \tag{1}$$

The constraint that no overlap may occur can be written as the set of inequalities,

$$\sqrt{(x_i-x_j)^2+(y_i-y_j)^2}\geq r_i+r_j\ \forall\ (i,j). \tag{2}$$

With an approach based on simulated annealing [2] and its variant [3] threshold accepting [4], we were able to produce the best known solutions for all system sizes considered in the benchmark contest [5].

While this benchmark is easy to formulate and seems rather specialized, it is nonetheless an exemplary problem of a multidisperse system of hard particles, which are widely used in physics: hard disks and hard spheres often serve as simple two-dimensional and three-dimensional models for granular matter, colloidal systems, fiber-reinforced composites, and molecular crystals [6–10]. Mostly, monodisperse and bidisperse systems are considered, i.e., either all disks and spheres exhibit the same radius value or one of two different values. But multidisperse packing problems exhibit additional fascinating properties when compared to monodisperse packing problems. The effect of multidispersity on the microstructure can be dramatic [11]. When considering, e.g., particles which partially exhibit conducting properties, one finds that they are often prevented from forming a connected network as a result of the relative size and composition of the surrounding nonconducting particles [12]. A further example involves the dissolution of a crystal comprised of multidisperse disks, where the large disks restrict the solubility of the crystal in the solvent [13].

We focus on this benchmark problem, as it has been proven to be non-deterministic polynomial time (NP)-complete, such that no exact algorithm solving this problem in polynomial time (there is no algorithm with exponent p and prefactor a for which the calculation time $t\leq aN^p$) exists, and as the benchmark contest provided world record results, with which we can compare our results. We use the general-purpose algorithm simulated annealing for optimizing this problem as it searches for a deep minimum in the energy landscape in an unbiased way. Besides the solution shown in Fig. 1 for $N=50$, we were able to find 9927 quasioptimum solutions with radius values $R<222$, which we already used in [5] for determining the neighborhood relations between the various disks. Analogously, we found vast numbers of quasioptimum solutions for the smaller system sizes considered in the contest. In this paper, we will show that the subspace of the quasioptimum configurations of this exemplary multidisperse packing problem exhibits the property of ultrametricity and will present computational results for the system size $N=50$.

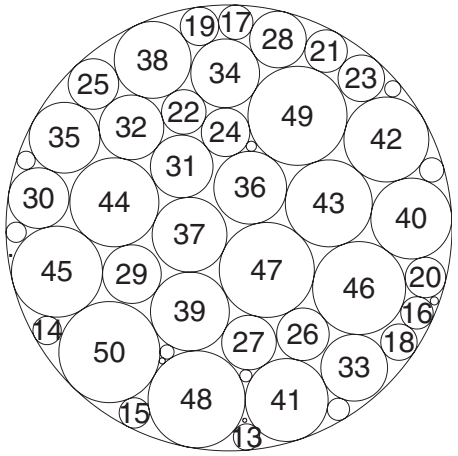

FIG. 1. Best solution found for the multidisperse packing problem with 50 disks: the circumcircle has a radius $R=220.600\,418\,7\ldots$. The numbers within the larger circles denote their radius values.

*schneidj@uni-mainz.de; URL: www.staff.uni-mainz.de/schneidj
†andmuell@uni-mainz.de
‡schoemer@uni-mainz.de; URL: www.staff.uni-mainz.de/schoemer

 ©2009 The American Physical Society

II. DEFINITION OF ULTRAMETRICITY

Starting with Parisi's investigation and solution of the Sherrington-Kirkpatrick (SK) model for spin glasses [14], not only this problem [15] but also other problems, such as the random-link traveling salesman problem (TSP) [16], have been investigated for whether their energy landscapes exhibit the property of ultrametricity [17], thus allowing for a deeper insight in the structure of these problems. It was conjectured that, generally, in frustrated optimization problems in which the imposed constraints cannot all be satisfied simultaneously, the optimal configurations spread in an ultrametric way in the configuration space [18], such that this ultrametricity property can be expected also to turn up in multidisperse packing problems. In order to determine ultrametric properties for the packing problem, we follow the approach used by Kirkpatrick and Toulouse [16] for the traveling salesman problem.

A standard metric is given by a function d, assigning each pair $(\vec{u},\vec{v})$ of points a real number $d(\vec{u},\vec{v})$ denoting the distance between them. In order to be a metric, the function d must obey to the constraints that

(1) $d(\vec{u},\vec{v}) \geq 0$ for all pairs $(\vec{u},\vec{v})$ of points (semipositive definiteness),

(2) $d(\vec{u},\vec{u})=0$ for all points $\vec{u}$, and

(3) $d(\vec{u},\vec{v}) \leq d(\vec{u},\vec{w})+d(\vec{w},\vec{v})$ (triangle inequality) for all triples $(\vec{u},\vec{v},\vec{w})$ of points.

If even $d(\vec{u},\vec{v})=d(\vec{v},\vec{u})$ for all pairs $(\vec{u},\vec{v})$ of points, then the metric is called symmetric. A standard example of a metric is the Euclidean metric,

$$d(\vec{u},\vec{v}) = \sqrt{\sum_{i=1}^{D} (u_i - v_i)^2} \tag{3}$$

in D dimensions. But there are also other important metrics such as the Manhattan metric, which reads as

$$d(\vec{u},\vec{v}) = \sum_{i=1}^{D} |u_i - v_i|, \tag{4}$$

and the Chebychev metric, which reads as

$$d(\vec{u},\vec{v}) = \max\{|u_i - v_i|\}. \tag{5}$$

These three examples belong to the class of $\mathcal{L}_p$-metrics, which can in general be written as

$$d(\vec{u},\vec{v}) = \left[\sum_{i=1}^{D} (u_i - v_i)^p \right]^{1/p}. \tag{6}$$

In case of an ultrametric, the triangle inequality (3) is replaced by the stricter ultrametricity condition,

$$d(\vec{u},\vec{v}) \leq \max\{d(\vec{u},\vec{w}),d(\vec{w},\vec{v})\}, \tag{7}$$

for all triples $(\vec{u},\vec{v},\vec{w})$ of points. When permuting $\vec{u}$, $\vec{v}$, and $\vec{w}$, one finds that the condition of ultrametricity is only fulfilled if the points $\vec{u}$, $\vec{v}$, and $\vec{w}$ form the edges of a triangle which is either equilateral or at least isosceles in the way that the base of the triangle is shorter than its legs.

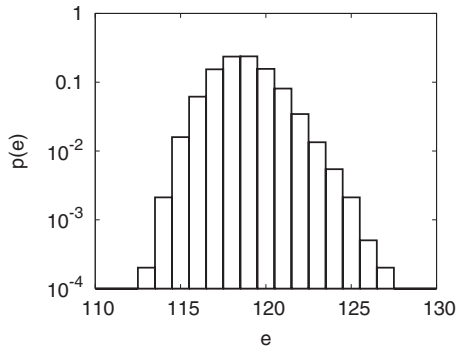

FIG. 2. Probability distribution of the number e of edges denoting the neighborhood relations between the various disks.

III. OVERLAPS BETWEEN CONFIGURATIONS

In the space of the configurations, points are simply given by configurations. A configuration of our multidisperse packing problem is given by the ordered set of coordinates of the midpoints of the N disks, $[(x_1,y_1),(x_2,y_2),(x_3,y_3),\ldots,(x_N,y_N)]$. For defining a function d, a similarity or dissimilarity measure between the configurations has to be defined. For this purpose, we use the neighborhood relations between various disks: we consider two disks i and j to be neighbors of each other if their corresponding cells in a Voronoi diagram [19,20] are adjacent to each other. Please note that the boundaries in the Voronoi diagram are not straight lines (as it would be the case if constructing Voronoi diagrams of sets of points or sets of disks with identical radii) but hyperbolic curves, as the radii r_i of the various disks differ. For very densely packed configurations, these hyperbolic curves are only slightly bent. By connecting the midpoints of disks in adjacent cells, we get a graph with edges, which comprise the Delaunay triangulation. Let η^σ be an edge matrix with

$$\eta^\sigma(i,j) = \begin{cases} 1 & \text{if the cells of disks } i \text{ and } j \text{ are adjacent to each other in configuration } \sigma \\ 0 & \text{otherwise.} \end{cases} \tag{8}$$

Then the overall number $e(\sigma)$ of edges in the configuration is simply given by

$$e(\sigma) = \frac{1}{2} \sum_{i,j} \eta^\sigma(i,j). \tag{9}$$

The minimum number of edges we find in the considered configurations is 113, the maximum is 127. The distribution of the number of edges, which is shown in Fig. 2, exhibits a sharp peak around its mean value $\langle e \rangle = 118.72$.

At this point, we may ask how much different solutions we have generally in common. For answering this question, we calculate the overlap between pairs of configurations. The un-normalized overlap $q_{\sigma\tau}$ between the configurations σ and τ is given as

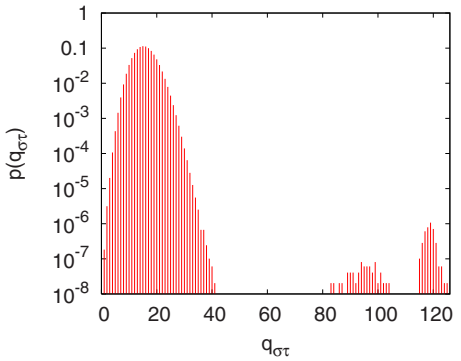

FIG. 3. (Color online) Probability with which a specific value of the overlap values $q_{\sigma\tau}$ is found for a pair of configurations (σ,τ) with $\tau \neq \sigma$.

$$q_{\sigma\tau} = \frac{1}{2}\sum_{i,j} \eta^{\sigma}(i,j)\,\eta^{\tau}(i,j). \tag{10}$$

One might want to normalize this overlap to

$$\tilde{q}_{\sigma\tau} = \frac{q_{\sigma\tau}}{\min\{e(\sigma),e(\tau)\}}, \tag{11}$$

but please note that the minimum number of edges varies slightly around its mean value $\langle \min\{e(\sigma),e(\tau)\}\rangle = 117.79$. Thus, we prefer to work with un-normalized overlaps, just as in the work of Kirkpatrick and Toulouse on the random-link traveling salesman problem in [18]. Throughout this paper, we will only work with overlap values which are not normalized and which we denote with the letter q. If we want to refer in some additional explanations to their corresponding normalized overlap values, we explicitly speak of normalized overlap values and denote them with $\tilde{q}$. We keep in mind that our corresponding normalized overlap values are restricted to the interval [0; 1], similar to the work of Kirkpatrick and Toulouse [18], thus, these are no algebraic numbers. Contrarily, when investigating configurations for spin-glass models, one gets normalized overlaps in the range [−1; 1].

Investigating these overlap values, we first create a histogram of the overlap values which occur between the $9923 \times 9922/2 = 49\,228\,003$ pairs (σ,τ) of configurations with $\tau \neq \sigma$. The probability with which the overlap values occur between our quasioptimum configurations is shown in Fig. 3. We find that there is no configuration, which is completely different from any other configuration, as $p(q=0)=0$. The largest overlap value is 125, which is rather close to the maximum number of edges occurring in a configuration, which was 127, as can be seen in Fig. 2. The mean value of the overlaps is $\langle q\rangle = 15.5754 \pm 5 \times 10^{-4}$. The maximum of the distribution lies at $q=15$, which 5 601 883 pairs of configurations have as overlap value. The distribution of the overlap values exhibits three peaks, one at $115 \leq q \leq 125$, a smaller one at $83 \leq q \leq 104$, and the largest one at $1 \leq q \leq 41$. Overlap values $q=85$, $q=88$, and in the ranges $42 \leq q \leq 82$ and $105 \leq q \leq 114$ do not occur. We checked those pairs of configurations with large overlap values in which way they differ from each other and found that the optimization runs generating these configurations ended basically up in the same solution, only differing in the locations of some of the smallest disks which are also called rattlers and which can be placed rather randomly in one of the holes between the jammed larger disks or close to the circumcircle. If using not all configurations with $R<222$ but selecting only those 378 solutions with $R<221.2$, only the left peak of the distribution remains, but it becomes narrower: the maximum overlap found is 24, the maximum of the peak is formed by 50 pairs of configurations with an overlap of 13. The vanishing of the middle and right subdistribution can be explained by the much smaller statistics here: the 378 configurations considered here were generated by independent optimization runs, leading to solutions which differ significantly from each other. In this smaller set of configurations, there is no pair of solutions anymore differing in the positions of a few rattlers only. Now we return to our overall set of 9923 solutions.

The overlaps define a distance measure between pairs of configurations. The relation between the normalized overlap $\tilde{q}_{\sigma\tau}$ and the distance $d(\sigma,\tau)$ between the configurations σ and τ is straightforward given as

$$d(\sigma,\tau) = 1 - \tilde{q}_{\sigma\tau}. \tag{12}$$

In terms of overlaps, we can rewrite the ultrametric condition (7) to

$$q_{\sigma\tau} \geq \min\{q_{\sigma\nu}, q_{\nu\tau}\} \tag{13}$$

and use the fact that overlaps are symmetric, i.e., $q_{\sigma\tau}=q_{\tau\sigma}$ for all pairs (σ,τ) of configurations.

IV. PARTIAL OVERLAP DISTRIBUTIONS

In order to prove the occurrence of the ultrametric property, we first determine the probability distribution $p(q_{\sigma\tau},q_{\tau\nu},q_{\nu\sigma})$ and consider the partial distribution $p(q_{\sigma\tau}=Q,q_{\tau\nu},q_{\nu\sigma})$ for a large fixed overlap value Q, for which $p(Q)$ is still sufficiently large to get a good statistics. If the condition of ultrametricity is fulfilled, then the histogram of $p(Q,q_{\tau\nu},q_{\nu\sigma})$ should exhibit a peak around the diagonal for all $q_{\tau\nu}=q_{\nu\sigma}\leq Q$. Figure 4 exemplarily shows the results for $Q=15$, for which the distribution of the overlap values exhibits its maximum, for $Q=25$, an overlap value which still lies in the left peak in the histogram shown in Fig. 3 and for which the probability is still sufficiently large, and for $Q=99$ and $Q=119$, at which the middle and the right peaks of the overlap histogram exhibit their maxima. We find indeed that the distribution exhibits a strong peak around the diagonal. For these and all other Q values, the maximum of the peak lies at $q_{\sigma\nu}=q_{\tau\nu}=15$. The overall maximum of the distribution is achieved for equilateral triangles with side length 15, which is not surprising, as the distribution of overlap values exhibits a strong peak at $q=15$, as shown in Fig. 3. However, as the location of the peak stays the same also for $Q<15$, the condition of ultrametricity is not well fulfilled there, as then the still likely occurring isosceles triangles have legs shorter than the base in terms of ultrametric distances. Furthermore, we note that the results differ for overlap values from different peaks in the overlap histogram: for small overlap values, the peaks are not very sharp, such that

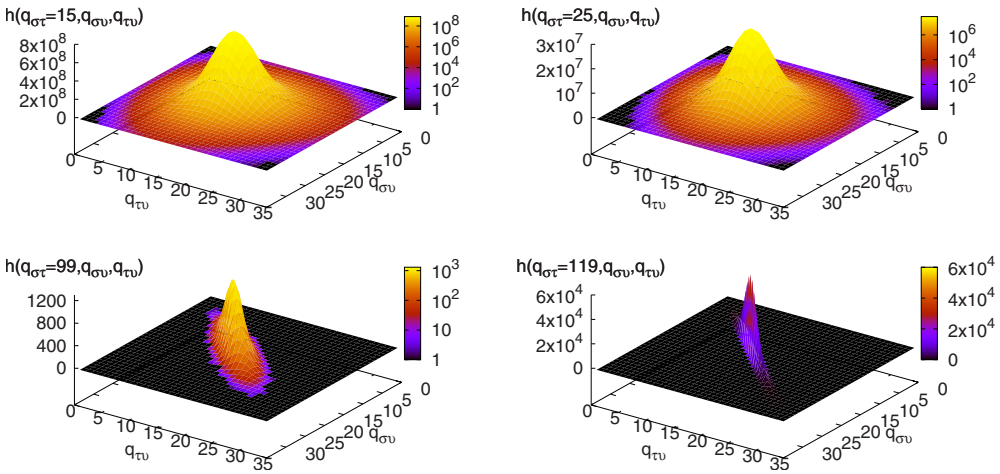

FIG. 4. (Color online) Un-normalized probability distribution $p(Q,q_{\sigma\upsilon},q_{\tau\upsilon})$ with $Q=15$ (top left), $Q=25$ (top right), $Q=99$ (bottom left), and $Q=119$ (bottom right): the histogram value $h(Q,q_{\sigma\upsilon},q_{\tau\upsilon})$ denotes how often a triangle with side lengths Q, $q_{\sigma\upsilon}$, and $q_{\tau\upsilon}$ was found.

triangles which are only roughly isosceles are also very likely. We see exemplarily for $Q=15$ and $Q=25$ that the peaks are approximately isotropically formed around the midpoint at $q_{\sigma\upsilon}=q_{\tau\upsilon}=15$. On the other hand, we find peaks which are long stretched around the diagonal but still centered around $q_{\sigma\upsilon}=q_{\tau\upsilon}=15$ for Q values from the second peak, as shown for $Q=99$. For Q values from the third peak, all nondiagonal histogram entries vanish entirely as the graphic for $Q=119$ shows exemplarily.

These three different regimes can be understood even better if performing a triangle statistics over all triples of configurations (σ,τ,υ), again with $\sigma\neq\tau\neq\upsilon\neq\sigma$. For each length $q_{\sigma\tau}$ of the base of a triangle, we measure the fractions $f_u(q_{\sigma\tau})$ of ultrametric triangles, $f_i(q_{\sigma\tau})$ of isosceles triangles, and $f_e(q_{\sigma\tau})$ of equilateral triangles. We find three different regimes for these fractions in Fig. 5, corresponding to the three peaks in the overlap distribution in Fig. 3: of course, no such fraction can be defined for overlap values which do not occur between pairs of configurations. In the regime $1\leq q_{\sigma\tau}\leq 41$, the fraction of ultrametric triangles sigmoidally approaches the fraction of isosceles triangles. Ultrametric triangles only occur for $q_{\sigma\tau}\geq 5$. The fraction of equilateral triangles is of course the smallest: equilateral triangles only occur for $5\leq q_{\sigma\tau}\leq 30$. f_e exhibits a slightly asymmetric peak at $q_{\sigma\tau}=15$. The fraction of ultrametric triangles first increases with the fraction of equilateral triangles with increasing $q_{\sigma\tau}$ and then approaches the fraction of isosceles triangles. f_u is equal to f_i for $q_{\sigma\tau}\geq 31$, i.e., all isosceles triangles are ultrametric. When neglecting small fluctuations, the fraction of isosceles triangles increases monotonously with increasing base length $q_{\sigma\tau}$. In the range of the second peak, the fractions of isosceles and ultrametric triangles again coincide. In the range of the third peak of the overlap distribution, i.e., for $115\leq q_{\sigma\tau}\leq 125$, we find that all triangles are ultrametric and isosceles. But please note that the statistics is worse for larger $q_{\sigma\tau}$ values: we have an overall maximum of $\sim 5.56\times 10^{10}$ triangles with base length $q_{\sigma\tau}=15$, but only overall 39 684 triangles for $q_{\sigma\tau}=99$ and 525 813 triangles for $q_{\sigma\tau}=119$. The minimum number of triangles of which the fractions f_u, f_i, and f_e are determined is of course 9921, for the case that a specific overlap value $q_{\sigma\tau}$ only occurs for one pair (σ,τ) of configurations. Therefore, the average values of our fractions are $\langle f_u\rangle=4.56\times 10^{-2}$, $\langle f_i\rangle=8.08\times 10^{-2}$, and $\langle f_e\rangle=7.53\times 10^{-3}$ and are thus dominated by the contributions at small values of $q_{\sigma\tau}$.

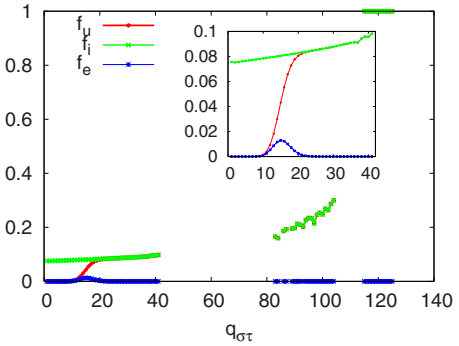

FIG. 5. (Color online) Fractions f_u of ultrametric triangles, f_i of isosceles triangles, and f_e of equilateral triangles for different base lengths $q_{\sigma\tau}$ of the triangles: the inset shows an enlargement of the curves at small values of $q_{\sigma\tau}$.

V. REMOVING THE INDEPENDENT BACKGROUND

However, simply counting the number of ultrametric triangles is not sufficient to determine the ultrametric property of a system. Instead, one has to remove the independent background [17]. For this purpose, let us first normalize the probability that a triangle with edge lengths $q_{\sigma\tau}=Q$, $q_{\sigma\upsilon}$, and $q_{\tau\upsilon}$ occurs according to

$$p(Q,q_{\sigma\upsilon},q_{\tau\upsilon})=\frac{h(Q,q_{\sigma\upsilon},q_{\tau\upsilon})}{\sum_{q_1,q_2}h(Q,q_1,q_2)}, \tag{14}$$

such that

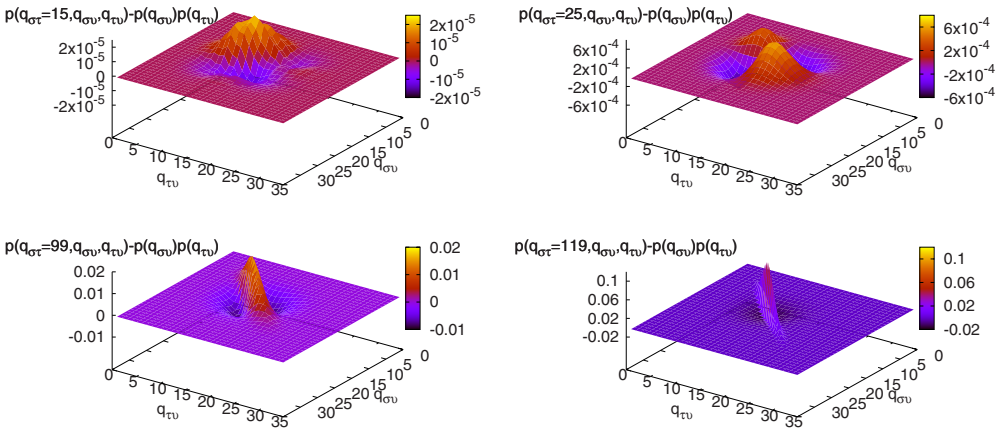

FIG. 6. (Color online) Ultrametricity measure $p(q_{\sigma\tau}=Q,q_{\sigma\nu},q_{\tau\nu})-p(q_{\sigma\nu})p(q_{\tau\nu})$ for $Q=15$ (top left), $Q=25$ (top right), $Q=99$ (bottom left), and $Q=119$ (bottom right).

$$\sum_{q_1,q_2} p(Q,q_1,q_2) = 1 \;\forall\; Q. \tag{15}$$

Then we define the probability $p(q_{\sigma\tau})$ that an edge with length $q_{\sigma\tau}$ occurs based on the histogram shown in Fig. 3. In the next step, we remove the independent background by subtracting the product $p(q_{\sigma\nu})p(q_{\tau\nu})$ from $p(Q,q_{\sigma\nu},q_{\tau\nu})$ for all values of Q. If the system exhibits the property of ultrametricity then we should see a positive peak stretched along the diagonal. But as Fig. 6 shows, we find a transition to a correct ultrametric behavior with increasing Q values: obviously, the peak of the histogram at $h(Q,Q,Q)$ for $Q=15$ in Fig. 4 was no sign for ultrametricity but only caused by the dominating overlap value of 15. If removing the background, only a very small positive entry remains, as shown in the top left graphic of Fig. 6. But other structures become more significant: for smaller overlap values, we find a small positive peak centered around the diagonal, for larger overlap values, a small negative peak. The picture changes when increasing Q: already for $Q=25$, we see two positive peaks centered around the diagonal and two negative peaks, left and right, besides the diagonal. Increasing the value of Q even further, the peak around the diagonal becomes long stretched and narrower. Additionally, we always find two small negative peaks located symmetrically around the diagonal.

There is also a second index for ultrametricity based on restricted probabilities [17]: let

$$\hat{h}(q_{\sigma\tau},q_{\sigma\nu},q_{\tau\nu}) = \begin{cases} h(q_{\sigma\tau},q_{\sigma\nu},q_{\tau\nu}) & \text{if } q_{\sigma\nu} \le q_{\sigma\tau} \\ & \text{and } q_{\tau\nu} \le q_{\sigma\tau} \\ 0 & \text{otherwise.} \end{cases} \tag{16}$$

Then we define the restricted probabilities,

$$r(Q,q_{\sigma\nu},q_{\tau\nu}) = \frac{\hat{h}(Q,q_{\sigma\nu},q_{\tau\nu})}{\sum_{q_1,q_2} \hat{h}(Q,q_1,q_2)}, \tag{17}$$

$$r(Q,q_{\sigma\nu}) = \frac{\sum_{q_2} \hat{h}(Q,q_{\sigma\nu},q_2)}{\sum_{q_1,q_2} \hat{h}(Q,q_1,q_2)}, \tag{18}$$

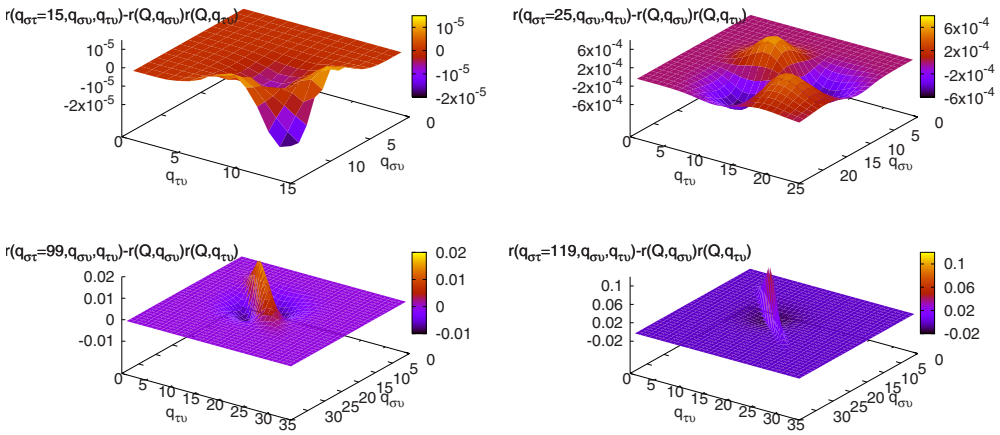

FIG. 7. (Color online) Ultrametricity measure $r(q_{\sigma\tau}=Q,q_{\sigma\nu},q_{\tau\nu})-r(Q,q_{\sigma\nu})r(Q,q_{\tau\nu})$ based on the restricted probabilities r (see text) for $Q=15$ (top left), $Q=25$ (top right), $Q=99$ (bottom left), and $Q=119$ (bottom right).

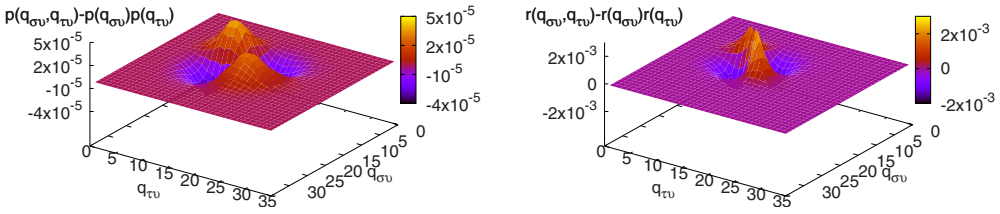

FIG. 8. (Color online) Ultrametricity measures $p(q_{\sigma\nu},q_{\tau\nu})-p(q_{\sigma\nu})p(q_{\tau\nu})$ (left) and $r(q_{\sigma\nu},q_{\tau\nu})-r(q_{\sigma\nu})r(q_{\tau\nu})$ (right) integrated over all $q_{\sigma\tau}$ values.

$$r(Q,q_{\tau\nu}) = \frac{\sum_{q_1} \hat{h}(Q,q_1,q_{\tau\nu})}{\sum_{q_1,q_2} \hat{h}(Q,q_1,q_2)}. \tag{19}$$

The results for this second measure are shown in Fig. 7. Please note that of course $r(Q,q_{\sigma\nu},q_{\tau\nu})=0$ if $q_{\sigma\nu}>Q$ or $q_{\tau\nu}>Q$. The largest difference to the previous measure shown in Fig. 6 is visible in the graphic for $Q=15$. The distribution for the restricted probabilities exhibits a strong negative peak at $q_{\sigma\nu}=q_{\tau\nu}=q_{\sigma\tau}=15$, whereas at this point, we find a slightly positive value in Fig. 6. With increasing Q, the graphics for this second measure shown in Fig. 7 gradually approach the corresponding graphics shown in Fig. 6.

We can of course go even a step further and integrate over all Q values, as described in [17], and then get the graphics for the two measures shown in Fig. 8.

Please note that looking at both measures is necessary: $p(q_{\sigma\nu},q_{\tau\nu})-p(q_{\sigma\nu})p(q_{\tau\nu})$ vanishes for a homogeneous distribution of points which provides a convenient null limit. But it vanishes also for a regular tree so that it does not test pure ultrametricity. Instead, it is sensitive to a combination of ultrametricity and heterogeneity. On the other hand, $r(q_{\sigma\nu},q_{\tau\nu})-r(q_{\sigma\nu})r(q_{\tau\nu})$ is more directly related to ultrametricity. For an ultrametric set of points, all positive values are concentrated on the diagonal. The drawback of this second measure is that it also gives a positive signal in the case of a homogeneous set of points. Thus, $p(q_{\sigma\nu},q_{\tau\nu})-p(q_{\sigma\nu})p(q_{\tau\nu})$ and $r(q_{\sigma\nu},q_{\tau\nu})-r(q_{\sigma\nu})r(q_{\tau\nu})$ provide complementary information and are thus both necessary to detect true ultrametricity. Summarizing, we find that the condition of ultrametricity is more likely fulfilled for a randomly chosen triangle, the longer the base of that triangle is.

VI. QUASIULTRAMETRICITY

In recent years, many scientists studying ultrametric properties of their systems have also started to consider the fractions of almost ultrametric triangles, e.g., by binning the underlying data to a very small set of representative values (see, e.g., [21]). These quasiultrametric triangles violate more or less the exact ultrametricity condition $q_{\sigma\tau} \geq \min\{q_{\sigma\nu},q_{\tau\nu}\}$ if considering the exact data values, but this approach of investigating quasiultrametricity is nevertheless interesting. We therefore have a look at the fraction $f_{\mathrm{qu}(\Delta q)}(q_{\sigma\tau})$ of quasiultrametric triangles with the base length $q_{\sigma\tau}$ and fulfilling the quasiultrametric properties,

$$|q_{\sigma\nu}-q_{\tau\nu}| \leq \Delta q,$$

$$q_{\sigma\nu} \leq q_{\sigma\tau}+\Delta q.$$

$$q_{\tau\nu} \leq q_{\sigma\tau}+\Delta q, \tag{20}$$

for $\Delta q \geq 0$. The results for these quasiultrametric fractions of triangles are shown in Fig. 9 for $\Delta q \leq 3$. Of course, the curve for $\Delta q=0$ reflects the correct ultrametricity condition and is therefore identical with the corresponding curve in Fig. 5. The larger the violation Δq, the larger of course the fraction of quasiultrametric triangles. But despite this increase in the fraction with increasing Δq, we find qualitatively the same increase in the fraction with increasing base length $q_{\sigma\tau}$ for various values of Δq.

VII. CONCLUSION AND OUTLOOK

In this paper, we considered a multidisperse system of N hard disks with different integer radii r_i $(1 \leq r_i \leq N)$, for which the densest packing in a circular environment had to be found. We solved this problem using simulated annealing, thus achieving a huge number of locally minimum quasioptimum configurations which we used to explore the structure of the energy landscape of these problems. We found that the set of quasioptimum solutions exhibits ultrametric properties.

We will extend our investigations to systems of hard spheres in three and even higher dimensions [22]. Then we will move on to other particle shapes, such as ellipsoids and spherocylinders. We expect to find the property of ultrametricity also for any other multidisperse packing problem with particles of different sizes, shapes, and/or interactions. Additionally, we will investigate further means to detect ultrametric properties of complex problems, e.g., by generating hierarchical trees, as the property of ultrametricity is directly linked to the possibility to create a hierarchical tree. A further approach would be to create a permutation ϕ of the configurations, thus reordering them in the way that we could get a matrix of normalized overlaps showing a block structure such as

$$(\tilde{q}_{\phi(\sigma),\phi(\tau)}) = \left(\begin{array}{cc|cc|cc} 1 & \tilde{q}_1 & & \tilde{q}_2 & & \\ \tilde{q}_1 & 1 & & & & \tilde{q}_3 \\ \hline & \tilde{q}_2 & 1 & \tilde{q}_1 & & \\ & & \tilde{q}_1 & 1 & & \\ \hline & & & & 1 & \tilde{q}_1 \\ & \tilde{q}_3 & & & \tilde{q}_1 & 1 \end{array}\right), \tag{21}$$

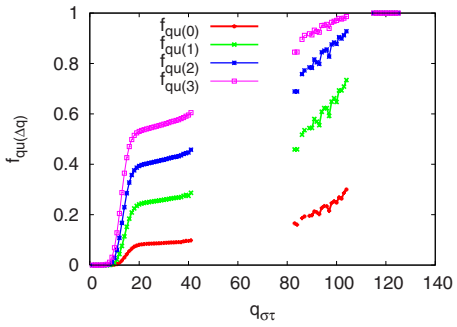

FIG. 9. (Color online) Fractions $f_{\mathrm{qu}(\Delta q)}(q_{\sigma\tau})$ of quasiultrametric triangles for increasing base length $q_{\sigma\tau}$, violating the exact ultrametric conditions by up to Δq units.

with normalized overlap values $1>\tilde{q}_1>\tilde{q}_2>\ldots$. This picture in formula (21) is given for the example of eight configurations, which, if located on a hierarchical tree, would form the leaves of a binary tree, such that we have ones in the diagonal, which denote the normalized overlap values of a configuration with itself, a relatively large normalized overlap value $\tilde{q}_1<1$ between pairs of neighboring configurations, a slightly smaller normalized overlap value $\tilde{q}_2$ between pairs of neighboring pairs, and so on. The structure of the matrix in Eq. (21) is related to the block structure used in the Parisi solution of the SK spin-glass model due to the iterated replica symmetry breaking. A way of obtaining such a permutation would be (when numbering all configurations and considering σ to be the number of the corresponding configuration) to maximize the objective function

$$\mathcal{H}(\phi) = \sum_{\sigma<\tau} \tilde{q}_{\phi(\sigma),\phi(\tau)} a^{|\phi(\sigma)-\phi(\tau)|}, \tag{22}$$

with the factor a being only slightly smaller than 1. First tests show that good results for this maximization problem can be achieved if applying simulated annealing [2] to this problem in combination with local search moves, which were developed for the TSP: the traveling salesman has the task to find the shortest closed tour through a given set of nodes, touching each node exactly once [23–25]. Analogously to the TSP, an optimum sequence has to be found, such that these problems are related to each other. Like for the TSP, we find that including higher-order moves, which cut not only two but three or four edges of the sequence and then reunite the partial sequences using new edges [26], improves the results considerably. Furthermore, the factor a should be gradually decreased during the optimization run, thus first emphasizing the generation of larger blocks and afterwards working out the local ordering inside the blocks. Like in further sequencing and other optimization problems [27–30], such blocks might turn up identically even in different quasioptimum solutions. Thus, we intend to apply the parallel searching for backbones algorithm [25,27,28] to this problem, which first generates a large number of quasioptimum solutions to this problem on the slave nodes, then lets the master node identify blocks common to these solutions, assumes these blocks to be optimally solved, and sends the information about these blocks back to the slaves, which perform new optimization runs holding these blocks constant. Thus, the effective size of the problem and therefore its complexity is significantly reduced, such that the slaves can concentrate on uniting the blocks in the optimum way. This approach is iterated until all slaves generate the same solution, which is hopefully the global optimum to this problem.

ACKNOWLEDGMENTS

This packing project was supported by the Forschungsfonds of the Johannes Gutenberg University of Mainz, the Collaborative Research Centre Transregio 6 (SFBTR6 under Subproject No. A5) of the German Research Foundation, and the newly founded Center for Computational Research Methods in Natural Sciences at the Johannes Gutenberg University of Mainz. Furthermore, we would like to thank the John von Neumann Institute for Computing (NIC) at the Research Center Julich, Germany, for a generous amount of computing time on the IBM Regatta under Project No. HMZ15 as well as the Center for Data Processing (ZDV) in Mainz. A.M. is very grateful to its administrator Markus Tacke for the introduction and his help with the computing facilities at the ZDV. Last but not least, J.J.S. gratefully acknowledges fruitful discussions with Uwe Krey (University of Regensburg, Germany) and Scott Kirkpatrick (The Hebrew University of Jerusalem, Israel) on the ultrametric properties of spin glasses and traveling salesman problems.

[1] http://www.recmath.org/contest/CirclePacking
[2] S. Kirkpatrick, C. D. Gelatt, Jr., and M. P. Vecchi, Science **220**, 671 (1983).
[3] P. Moscato and J. F. Fontanari, Phys. Lett. A **146**, 204 (1990).
[4] G. Dueck and T. Scheuer, J. Comput. Phys. **90**, 161 (1990).
[5] A. Müller, J. J. Schneider, and E. Schömer, Phys. Rev. E **79**, 021102 (2009).
[6] H. Reiss, H. M. Ellerby, and J. A. Manzanares, J. Phys. Chem. **100**, 5970 (1996).
[7] W. B. Russel, D. A. Saville, and W. R. Schowalter, *Colloidal Dispersions* (Cambridge University Press, Cambridge, England, 1989).
[8] S. Torquato and F. Lado, Proc. R. Soc. London, Ser. A **417**, 59 (1988).
[9] G. Metcalfe, T. Shinbrot, J. J. McCarthy, and J. M. Ottino, Nature (London) **374**, 39 (1995).
[10] R. Zallen, *The Physics of Amorphous Solids* (Wiley, New York, 1983).
[11] O. U. Uche, F. H. Stillinger, and S. Torquato, Physica A **342**, 428 (2004).
[12] S. Torquato, *Random Heterogeneous Materials: Microstructure and Macroscopic Properties* (Springer, New York, 2002).
[13] B. Mahan and R. Myers, *University Chemistry* (Benjamin/Cummings, Menlo Park, CA, 1987).

[14] D. Sherrington and S. Kirkpatrick, Phys. Rev. Lett. **35**, 1792 (1975).
[15] M. Mezard, G. Parisi, N. Sourlas, G. Toulouse, and M. A. Virasoro, J. Phys. (France) **45**, 843 (1984).
[16] S. Kirkpatrick and G. Toulouse, J. Phys. (France) **46**, 1277 (1985).
[17] R. Rammal, G. Toulouse, and M. A. Virasoro, Rev. Mod. Phys. **58**, 765 (1986).
[18] J. P. Bouchaud and P. Le Doussal, Europhys. Lett. **1**, 91 (1986).
[19] J. O'Rourke, *Computational Geometry in C*, 2nd ed. (Cambridge University Press, Cambridge, 1998).
[20] M. de Berg, O. Cheong, M. van Kreveld, and M. Overmars, *Computational Geometry: Algorithms and Applications*, 3rd ed. (Springer, Berlin, 2008).
[21] F. Murtagh, Eur. Phys. J. B **43**, 573 (2005).
[22] A. Müller, J. J. Schneider, and E. Schömer (unpublished).
[23] G. Reinelt, *The Traveling Salesman* (Springer, Berlin, 1994).
[24] E. L. Lawler, J. K. Lenstra, A. H. G. Rinnoy Kan, and D. B. Shmoys, *The Traveling Salesman Problem* (Wiley, New York, 1985).
[25] J. J. Schneider and S. Kirkpatrick, *Stochastic Optimization* (Springer, Berlin, 2006).
[26] G. Stattenberger, M. Dankesreiter, F. Baumgartner, and J. J. Schneider, J. Stat. Phys. **129**, 623 (2007).
[27] J. Schneider, Ch. Froschhammer, I. Morgenstern, Th. Husslein, and J. M. Singer, Comput. Phys. Commun. **96**, 173 (1996).
[28] J. Schneider, FGCS, Future Gener. Comput. Syst. **19**, 121 (2003).
[29] J. Schneider, J. Britze, A. Ebersbach, I. Morgenstern, and M. Puchta, Int. J. Mod. Phys. C **11**, 949 (2000).
[30] J. J. Schneider, in *Third International Symposium on Slow Dynamics in Complex Systems, Sendai, Japan, 3–8 November 2003*, edited by M. Tokuyama and I. Oppenheim, AIP Conf. Proc. No. 708 (AIP, New York, 2004), pp. 426–429.